Supporting Information for: Intermolecular $^{119}Sn,^{31}P$ Through-Space Spin-Spin Coupling in a Solid Bivalent Tin Phosphido Complex

Janet Arras,[†,‡] Klaus Eichele,[†] Boris Maryasin,[‡] Hartmut Schubert,[†]

Christian Ochsenfeld,[*,‡] and Lars Wesemann[*,†]

†*Institut für Anorganische Chemie, Universität Tübingen, Auf der Morgenstelle 18, 72076 Tübingen, Germany*

‡*Theoretische Chemie, University of Munich (LMU Munich), Butenandtstraße 7, 81377 Munich, Germany*

E-mail: christian.ochsenfeld@uni-muenchen.de; lars.wesemann@uni-tuebingen.de

Contents

1 Experimental Section

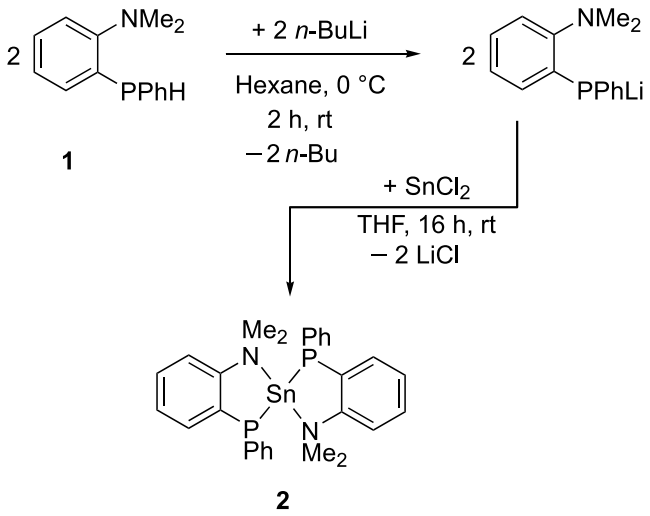

Scheme S1: Synthesis of the Bisamino Bisphosphide Tin Complex $Sn(NP)_2$, **2**, from the Secondary Phosphine NPH, **1**.

1.1 General Procedures

All reactions were performed under an argon atmosphere in an MBraun glovebox or by using standard Schlenk line techniques. Chemicals were purchased commercially and used without further purification except for NPH = $(2\text{-}Me_2NC_6H_4)PH(C_6H_5)$, **1**, which was synthesized according to a published procedure.[1] All nondeuterated solvents were purified by established methods and stored under argon. $[D_8]$Toluene and $[D_8]$tetrahydrofuran were degassed by three freeze-pump-thaw cycles and stored over sodium or molecular sieve, respectively. Unless otherwise stated, ^{1}H, $^{13}C\{^{1}H\}$ and $^{31}P\{^{1}H\}$ NMR characterization data were obtained at 299 K by using a Bruker AVII+400 NMR spectrometer (equipped with a 5 mm QNP probe head and operating at 400.13, 100.6 and 162.0 MHz, respectively). $^{119}Sn\{^{1}H\}$ NMR characterization data were obtained at 299 K using a Bruker DRX-250 NMR spectrometer (equipped with a 5 mm ATM BBO probe head and operating at 93.3 MHz). Chemical shifts (δ) are reported

in parts per million relative to external $SiMe_4$ (for ^1H and ^{13}C), 85% H_3PO_4 in D_2O (for ^{31}P) and $SnMe_4$ (for ^{119}Sn) by using the chemical shift of the solvent ^2H resonance frequency in combination with the unified frequency scale according to paragraph 3.6 of the IUPAC 2001 recommendations.[2] Variable-temperature NMR spectroscopic data were collected with a Bruker Avance II+500 spectrometer (equipped with a 5 mm ATM BBO probe head and operating at 500.13 (^1H), 125.8 (^{13}C), 202.5 (^{31}P) and 186.6 (^{119}Sn) MHz, respectively). ^1H and ^{13}C NMR chemical shift assignments are based on data obtained from ^1H-^1H COSY, ^1H-^1H NOESY, ^1H-^{13}C HSQC and ^1H-^{13}C HMBC NMR experiments. The solid-state ^{31}P and ^{119}Sn CP/MAS spectra were obtained at 81.0 and 74.7 MHz by using a Bruker DSX-200 super wide bore spectrometer (B_0 = 4.7 T). Powdered samples of **2** were packed into 4 mm zirconia rotors. After cross-polarization (CP), the spectra were acquired under high-power proton decoupling and were referenced to external 85% H_3PO_4 (for ^{31}P) and $SnMe_4$ (for ^{119}Sn) by setting external $NH_4H_2PO_4$ to 0.81 ppm or $SnCy_4$ to −97.35 ppm.[3] Elemental analyses were performed by the Institut für Anorganische Chemie, University of Tübingen with a Vario MICRO EL analyzer from Elementar Co.

1.2 Synthesis of Li[(2-$Me_2NC_6H_4$)P(C_6H_5)], Li(NP)

To a solution of (2-$Me_2NC_6H_4$)PH(C_6H_5) (20.0 mg, 0.09 mmol) in 15 mL *n*-hexane 0.04 mL of *n*-BuLi (0.09 mmol; 2.5 M in *n*-hexane) was added drop wise. The resulting suspension was stirred at RT for 2 h. Subsequently, the volatile components were removed in vacuo and the yellow solid of Li(NP) was dried.

^{31}P NMR (162.0 MHz, THF-d_8): $\delta = -43.6$ [s].

1.3 Synthesis of [Sn(NP)$_2$], 2

To a mixture of $SnCl_2$ (9.5 mg, 0.05 mmol) and 7 mL of THF (distilled) was added drop wise a THF (distilled) solution of Li(NP) (23.8 mg, 0.10 mmol; in 7 mL). The resulting solution was stirred at RT for 16 h and filtered. The volatile components were removed in vacuo, extracted with *n*-hexane (distilled) and filtered. The solvent was removed in vacuo. After extraction in THF (distilled), yellow single crystals of **2** can be obtained by slow evaporation of the solvent (14.0 mg; 85% yield).

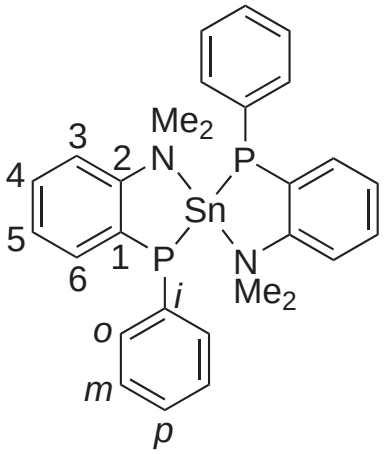

Figure S1: Labeling for assignment of NMR spectra of [Sn(NP)$_2$], **2**

^{1}H NMR (500.13 MHz, C_6D_6): δ = 1.70 [br s, 6 H, NMe^A], 2.72 [br s, 6 H, NMe^B], 6.58 [m, 2 H, H-3], 6.78, 6.80 [m, 4 H, H-4,5], 7.00 [m, 2 H, p-H], 7.07 [m, 4 H, m-H], 7.50 [m, 2 H, H-6], 7.86 [m, 4 H, o-H]. **^{13}C{^{1}H} NMR** (125.77 MHz, C_6D_6): δ = 44.8 [br, $N(CH_3)_2$], 48.5 [br, $N(CH_3)_2$], 117.5 [s, C3], 125.3, 125.4 [s, C4,5], 127.3 [s, *p*-C], 128.3 [m, *m*-C], 135.5 [s, C6], 137.8 [m, *o*-C, *N* = 18.0 Hz], 142.4 [m, *i*-C, *N* = 29.1 Hz], 142.9 [m, C1, *N* = 17.4 Hz], 152.2 [m, C2, *N* = 8.6 Hz]. **^{31}P{^{1}H} NMR** (162.0 MHz, Tol-d_8): $\delta = -55.1$ [s + d, $^1J(^{119}Sn,^{31}P)$ = 834 Hz, $^1J(^{117}Sn,^{31}P)$ = 799 Hz]. **^{119}Sn{^{1}H} NMR** (93.3 MHz, Tol-d_8): δ = 410.5 [t, $^1J(^{119}Sn,^{31}P)$ = 834 Hz].

Elemental analysis (%) calcd. for $C_{28}H_{30}N_2P_2Sn$: C, 58.47; H, 5.26; N, 4.87. Found: C, 58.29; H, 5.46; N, 4.71.

1.4 Solution NMR Spectroscopy

The solution NMR spectra shown in this section result from a sample that has been stored in a glove box under Argon for two years. The free ligand, NPH,[1] is a frequent impurity (decomposition product) for this type of compound, cf. Izod et al.,[4] and the peaks arising from NPH are marked in the following spectra by an asterisk.

Included here are the following solution NMR spectra:

- ^{1}H NMR spectrum: Fig. S2, p. S7
- ^{1}H COSY-45 NMR spectrum: Fig. S3, p. S8
- ^{1}H NOESY NMR spectrum: Fig. S4, p. S9
- ^{13}C{^{1}H} NMR spectrum: Fig. S5, p. S10
- ^{1}H,^{13}C HSQC und HMBC NMR spectra: Fig. S6, p. S11

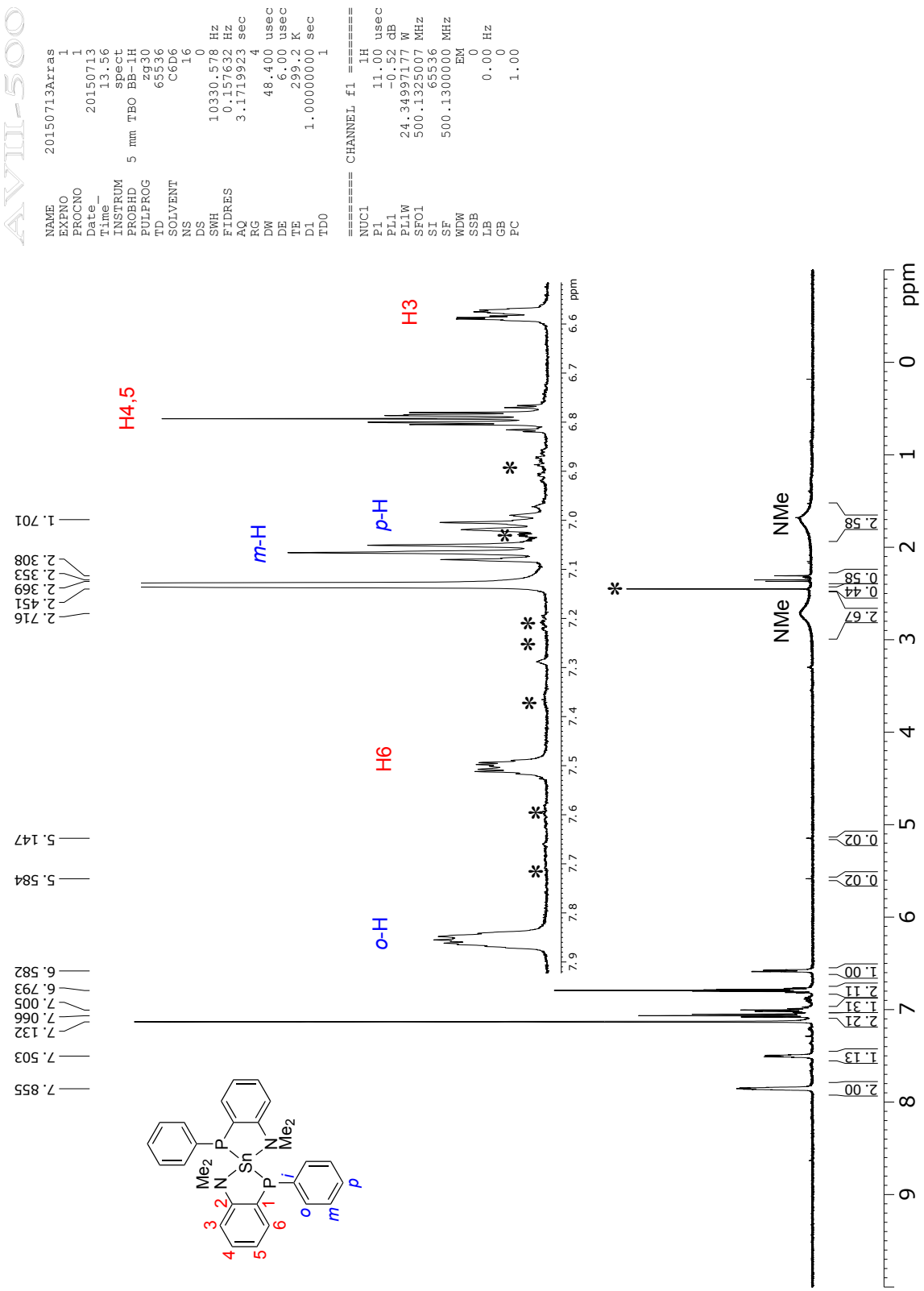

Figure S2: ^{1}H NMR spectrum of [Sn(NP)$_2$], **2**, in C_6D_6, obtained at $B_0 = 11.75$ T. Peaks from NPH are marked by an asterisk.

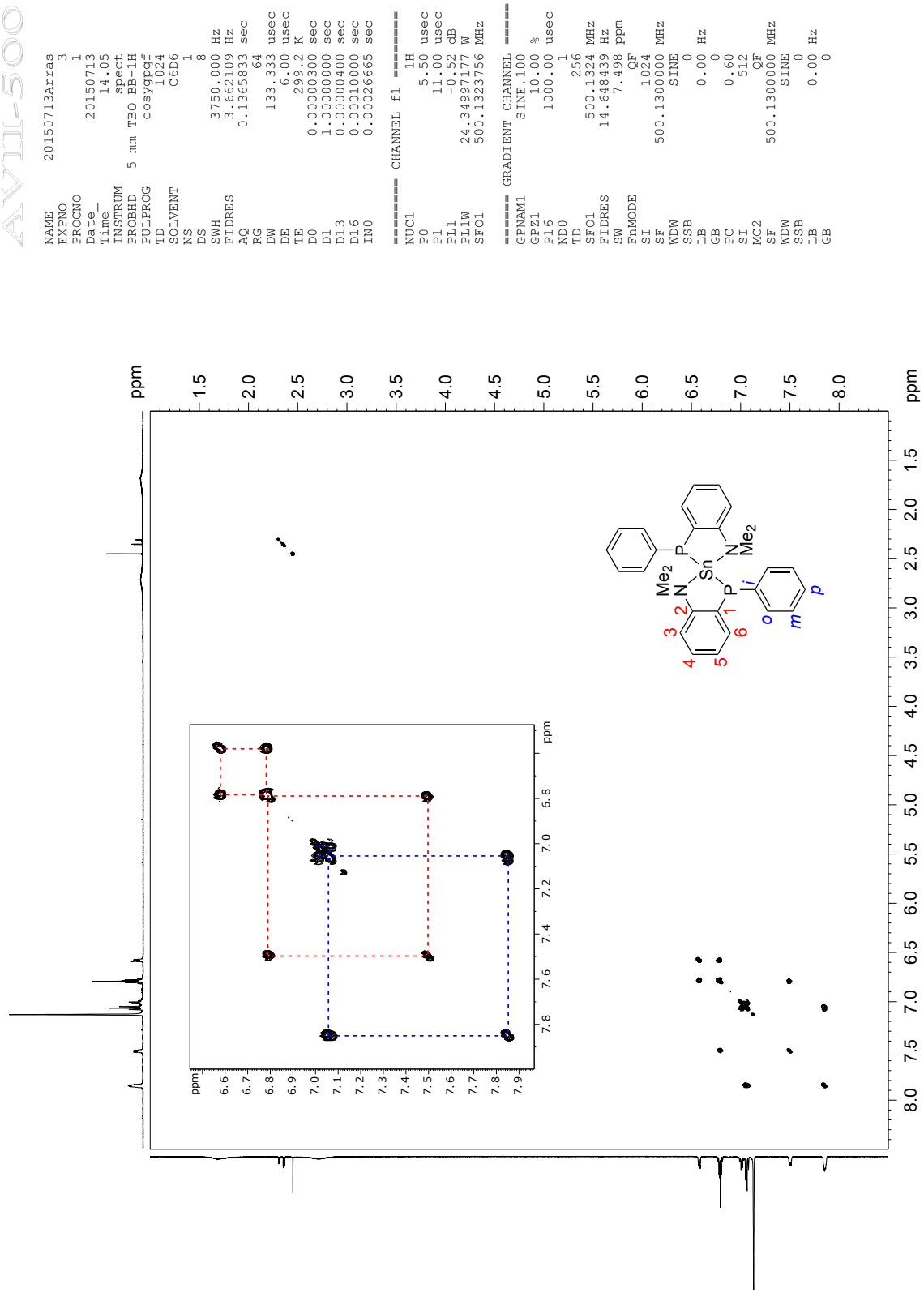

Figure S3: ^{1}H COSY-45 NMR spectrum of [Sn(NP)$_2$], **2**, in C_6D_6, obtained at $B_0 = 11.75$ T.

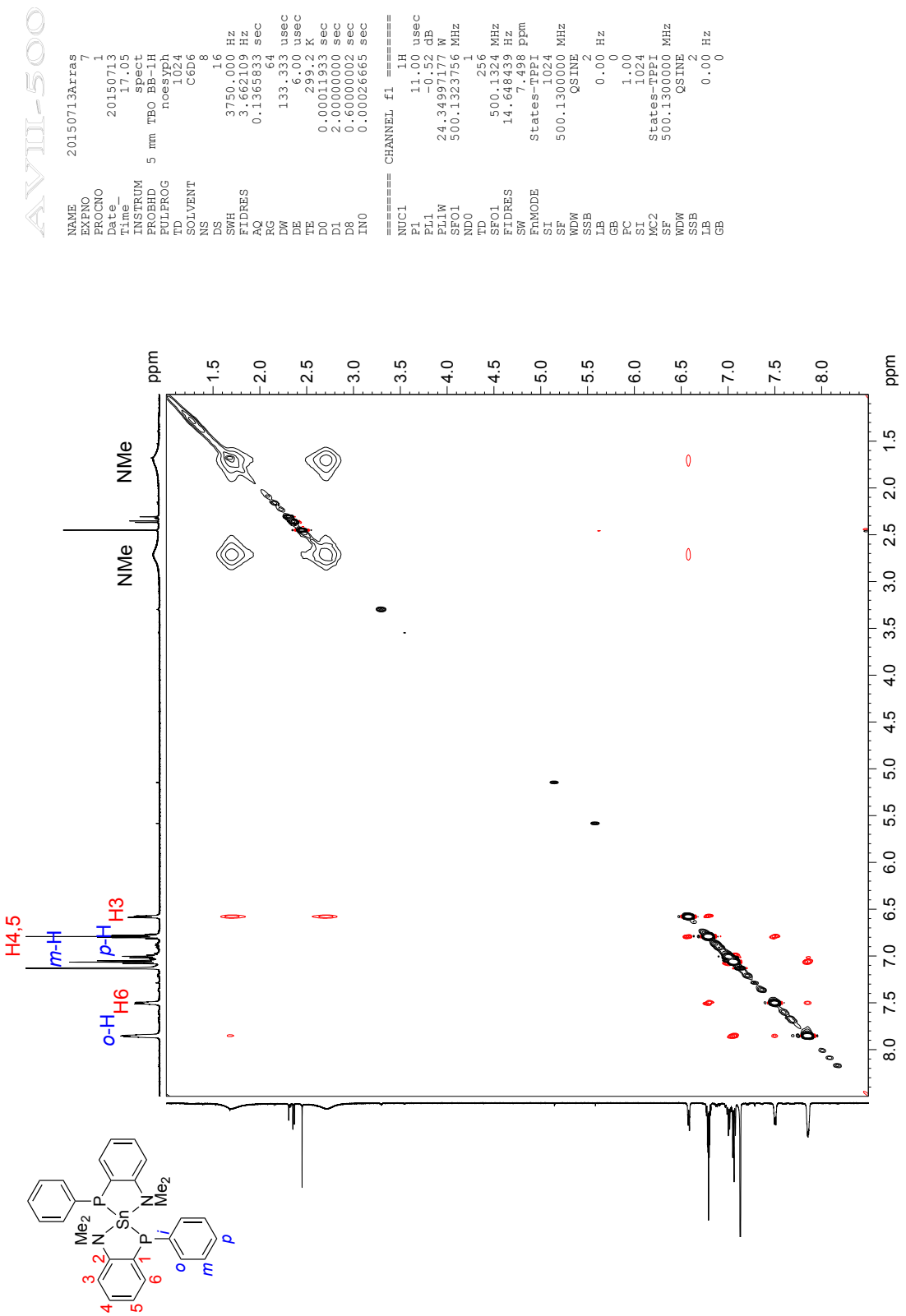

Figure S4: ^{1}H NOESY NMR spectrum of [Sn(NP)$_2$], **2**, in C_6D_6, obtained at $B_0 = 11.75$ T.

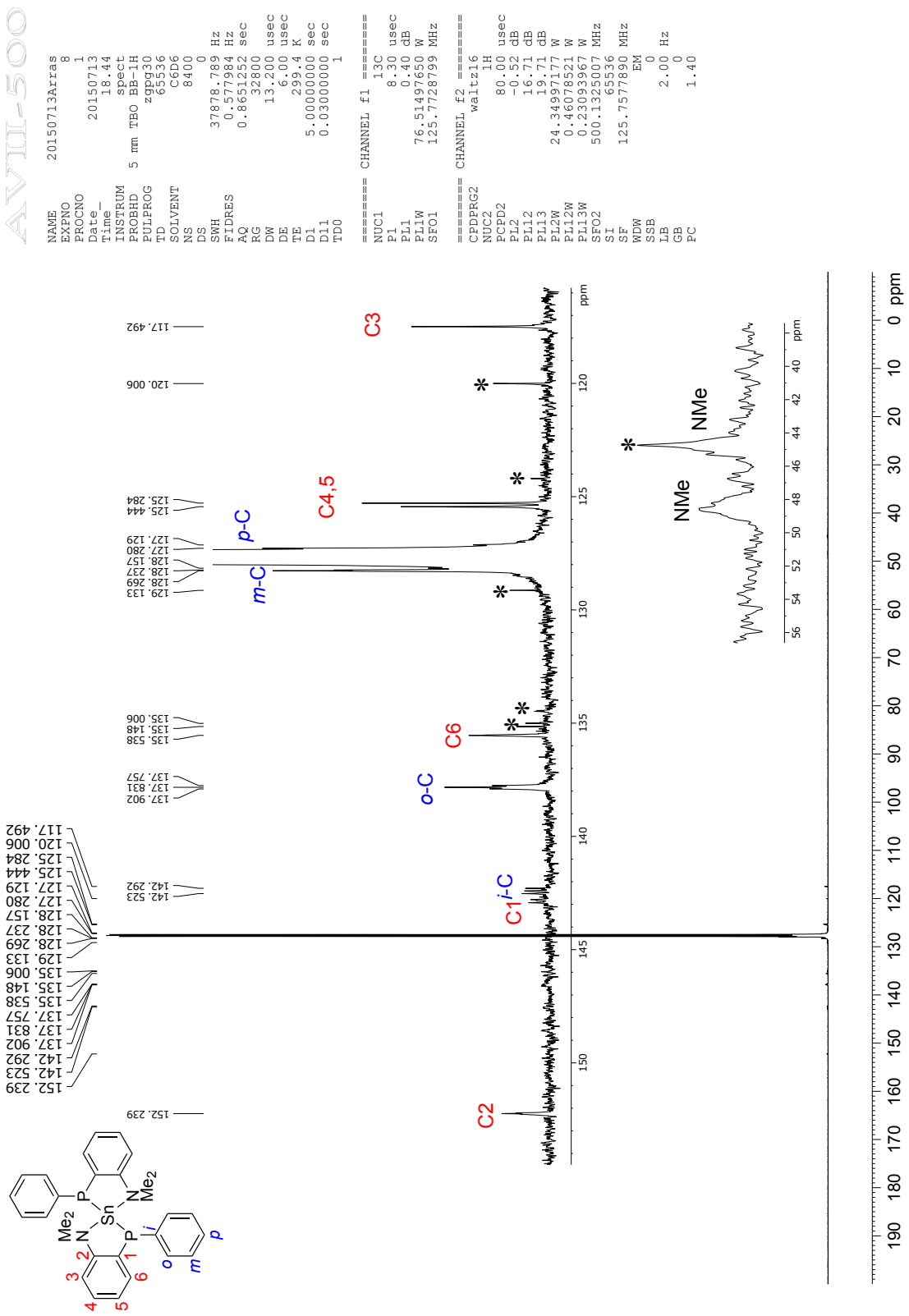

Figure S5: $^{13}C\{^1H\}$ NMR spectrum of [Sn(NP)$_2$], **2**, in C_6D_6, obtained at $B_0 = 11.75$ T. Peaks from NPH are marked by an asterisk.

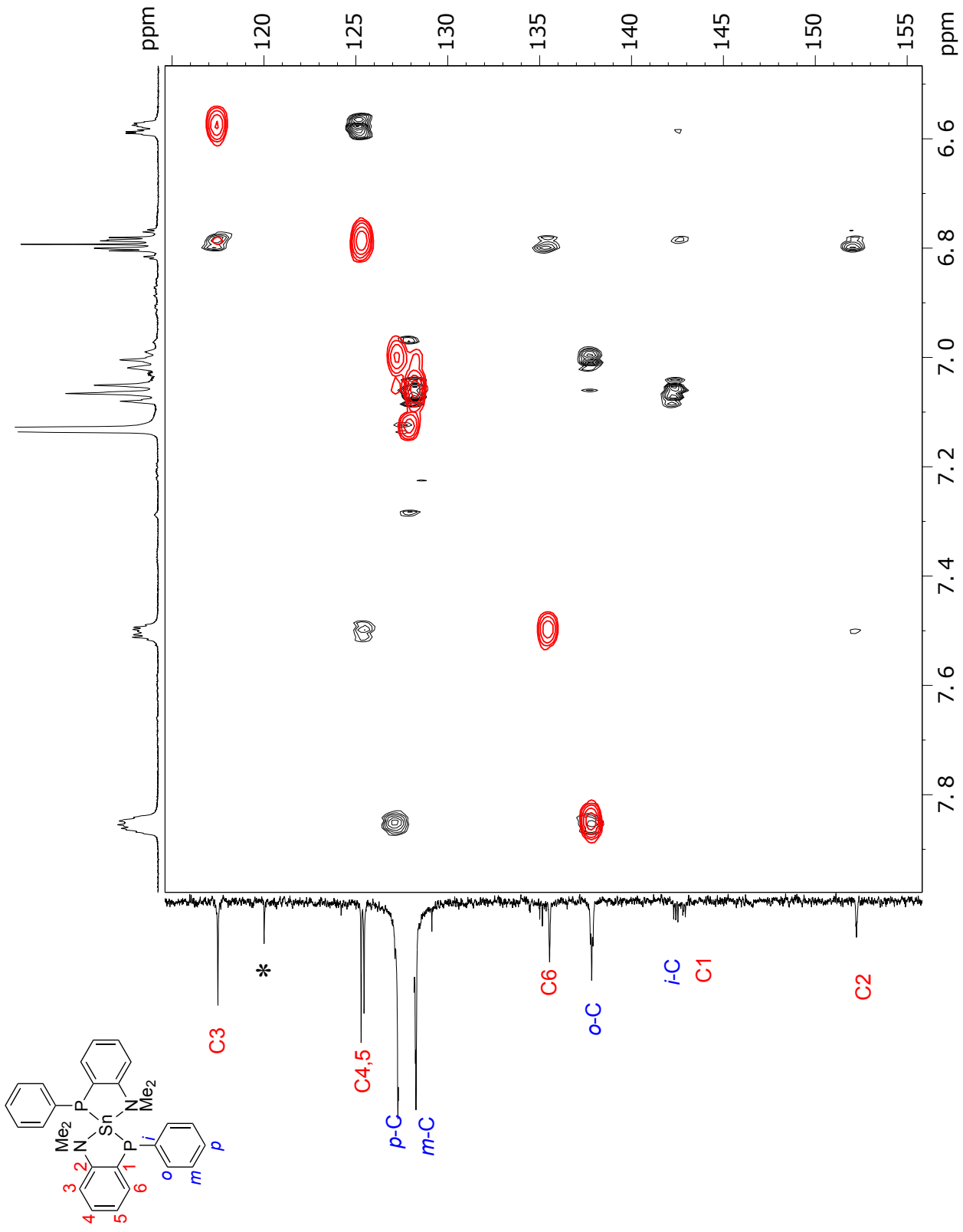

Figure S6: Overlay of ^{1}H,^{13}C HSQC (red contours) and HMBC (black contours) NMR spectra of [Sn(NP)$_2$], **2**, in C_6D_6, obtained at $B_0 = 11.75$ T. Peaks from NPH are marked by an asterisk.

1.5 Solid-State NMR Spectroscopy

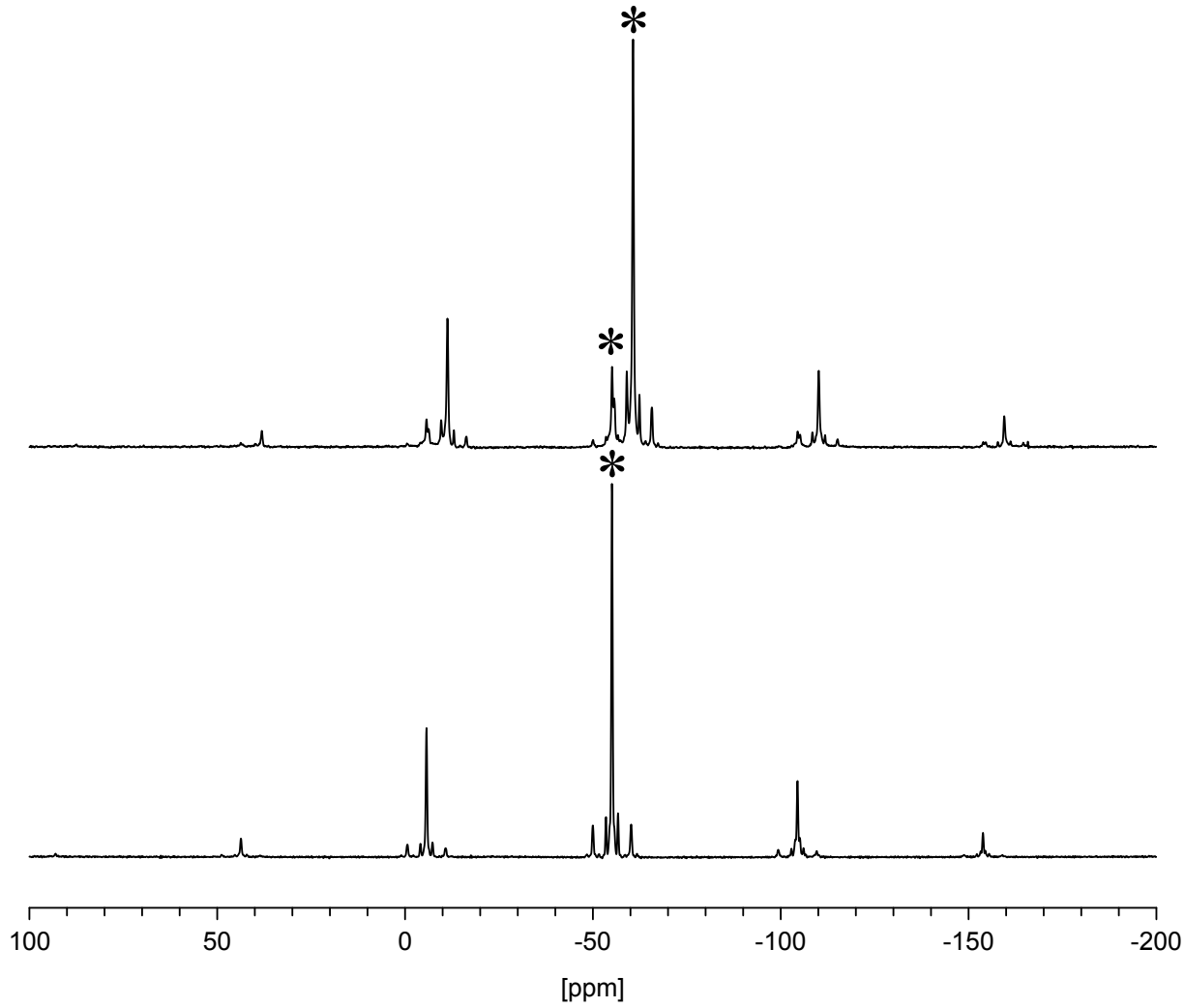

Figure S7: ^{31}P CP/MAS NMR spectra of [Sn(NP)$_2$], **2**, precipitated by addition of *n*-hexane to a THF solution (top), or crystallized from THF (bottom). Spinning rate: 4 kHz, $B_0 = 4.7$ T. The isotropic peaks are indicated by asterisks.

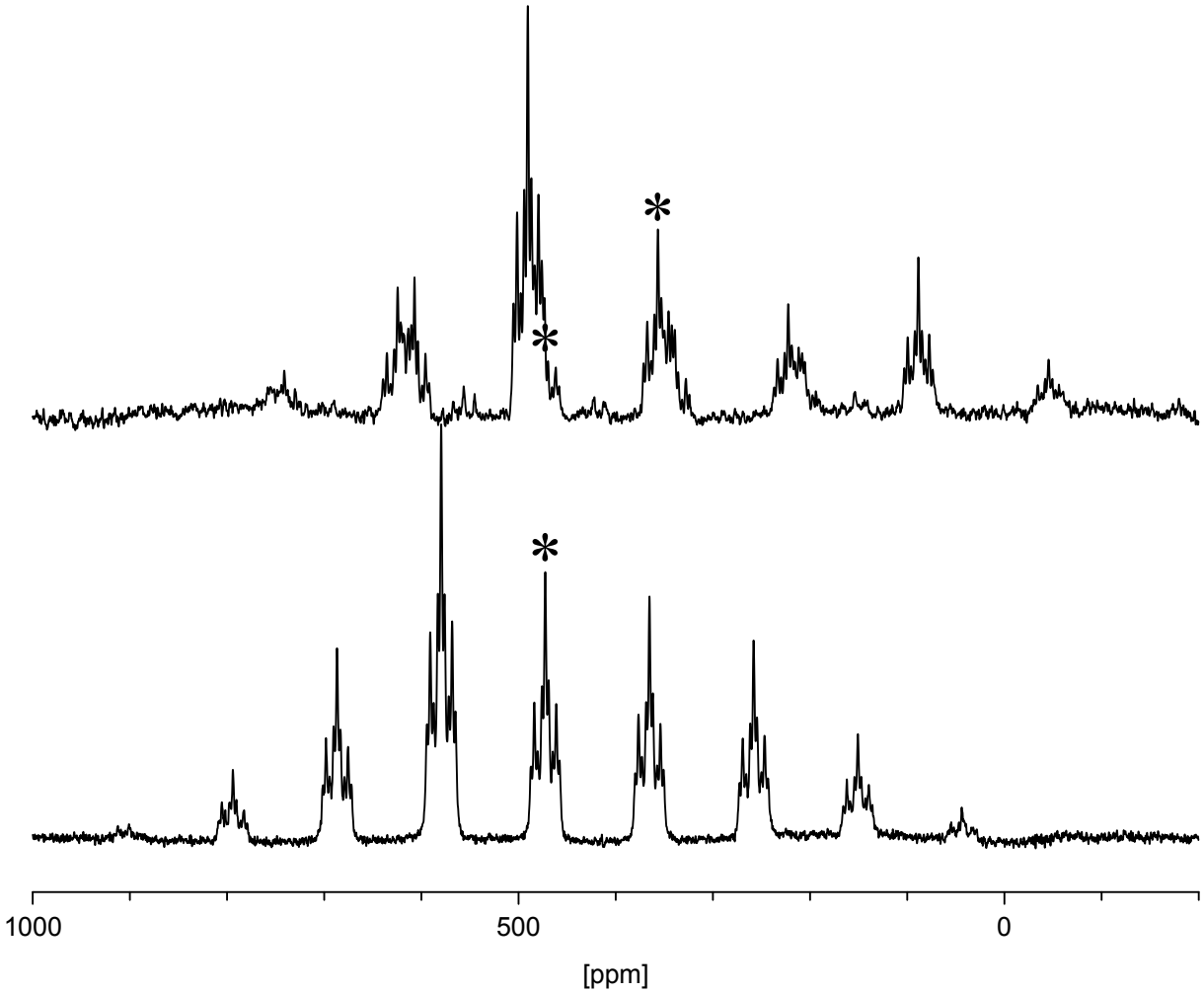

Figure S8: ^{119}Sn CP/MAS NMR spectra of [Sn(NP)$_2$], **2**, precipitated by addition of *n*-hexane to a THF solution (top, spinning rate 10 kHz), or crystallized from THF (bottom, spinning rate 8 kHz). $B_0 = 4.7$ T. The isotropic peaks are indicated by asterisks.

1.6 Structural Characterization

Details of the single-crystal X-ray diffraction experiments on $Sn(NP)_2$ from THF, **2(thf)**, and from *n*-hexane, **2(hex)**, can be found in the accompanying CIF file. Some results are summarized below.

1.6.1 $Sn(NP)_2$ from THF, 2(thf)

The X-ray data for **2(thf)** were collected with a Bruker AXS diffractometer. The integration was done with the Bruker SAINT software package by using a narrow-frame algorithm.[5] Absorption correction was applied by using the multiscan method (SADABS).[6] The structure was solved and refined by using the SHELXTL software package and the WinGX program suite.[7] All hydrogen atoms were placed in calculated positions and refined with isotropic displacement parameters.

$C_{28}H_{30}N_2P_2Sn$, M_r = 575.19 g mol^{-1}, yellow, λ = 0.71073 Å, T = 100(2) K, tetragonal space group $I\,4_1$ cd, Z = 8, a = 21.082(2) Å, b = 21.082(2) Å, c = 11.5882(12) Å, α = 90°, β = 90 °, γ = 90 °, V = 5150.4(9) Å^3, ρ_{calc}= 1.483 g cm^{-3}, μ = 1.135 mm^{-1}, $F(000)$ = 2336, θ range = 6.73 –27.56°, 2318 independent reflections, R_1 = 0.0175, wR_2 [I $> 2\sigma$(I)] = 0.0268, R_1 = 0.0278, wR_2 (all data) = 0.0279 and 152 parameters.

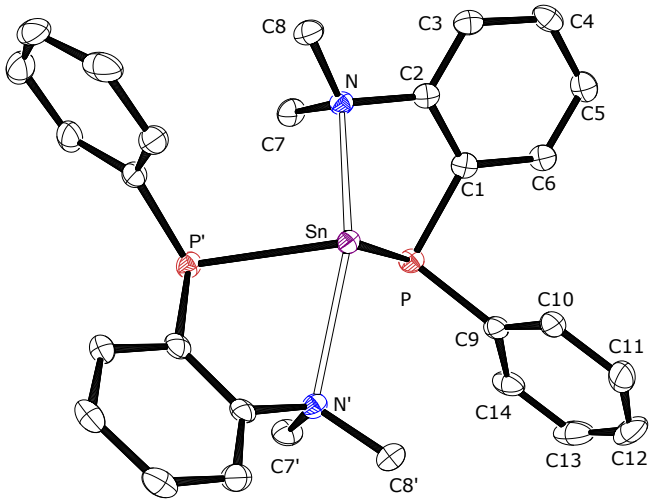

Figure S9: Molecular structure (ORTEP diagram shown with 50% displacement ellipsoids) of complex **2(thf)** crystallized from THF) in the solid state. Hydrogen atoms have been omitted for clarity.

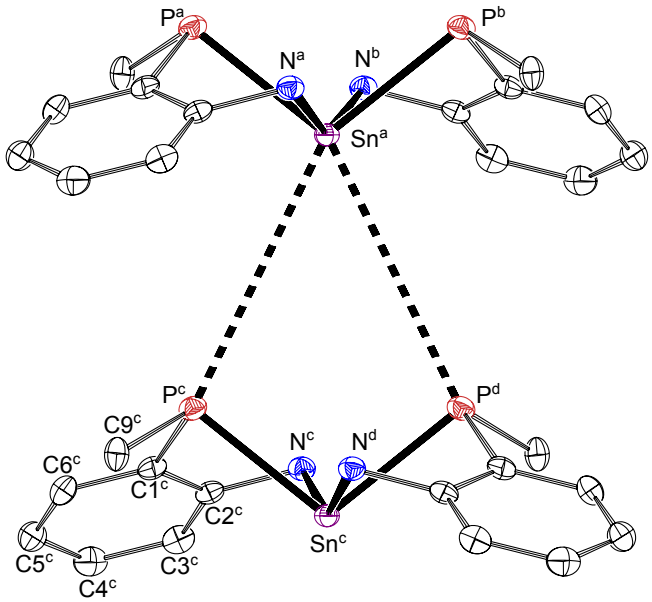

Figure S10: Two molecules of **2** crystallized from THF, **2(thf)**; hydrogen atoms, phenyl carbons except for ipso and methyl groups have been omitted. The superscripts to the atom labels correspond to the following symmetry operations: *a* (x, 2−y, $-\frac{1}{2}$z); *b* (2−x, y, $-\frac{1}{2}$+z); *c* (x, y, z); *d* (2−x, 2−y, z).

1.6.2 $Sn(NP)_2$ from *n*-hexane, 2(hex)

The X-ray data for **2(hex)** were collected with a Stoe IPDS 2T diffractometer and were corrected for Lorentz and polarization effects and absorption by air. The programs used in this work are Stoe X-Area[8] and the WinGX suite of programs,[7] which includes SHELXS and SHELXL for structure solution and refinement.[9,10]

$C_{28}H_{30}N_2P_2Sn$, M_r = 575.19 g mol^{-1}, yellow, λ = 0.71073 Å, T = 173 K, tetragonal space group $P\,4_2/n$, Z = 4, a = 14.8396(3) Å, b = 14.8396(3) Å, c = 11.7863(3) Å, α = 90°, β = 90°, γ = 90°, V = 2595.51(12) Å^3, ρ_{calc} = 1.472 g cm^{-3}, μ = 1.127 mm^{-1}, $F(000)$ = 1168, θ range = 3.88–29.19°, 3040 independent reflections, R_1 = 0.0283, wR_2 [I > 2σs(I)] = 0.0593, R_1 = 0.0357, wR_2(all data) = 0.0622 and 150 parameters.

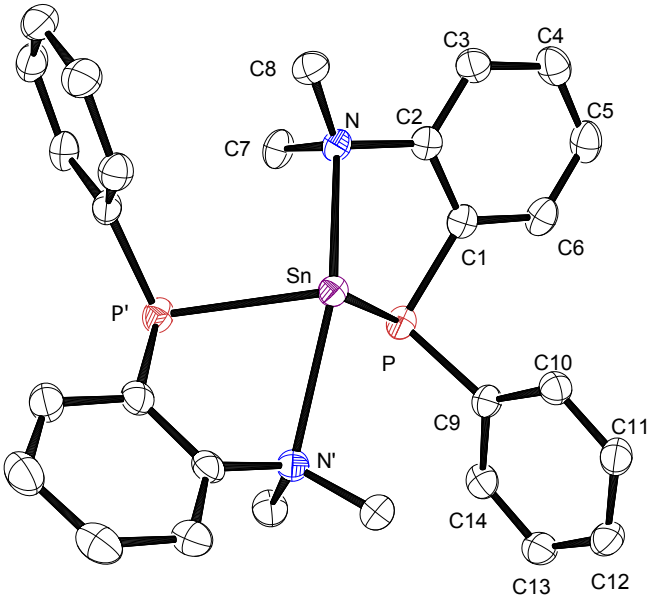

Figure S11: Molecular structure (ORTEP diagram shown with 50% displacement ellipsoids) of complex **2(hex)** crystallized from *n*-hexane) in the solid state. Hydrogen atoms have been omitted for clarity.

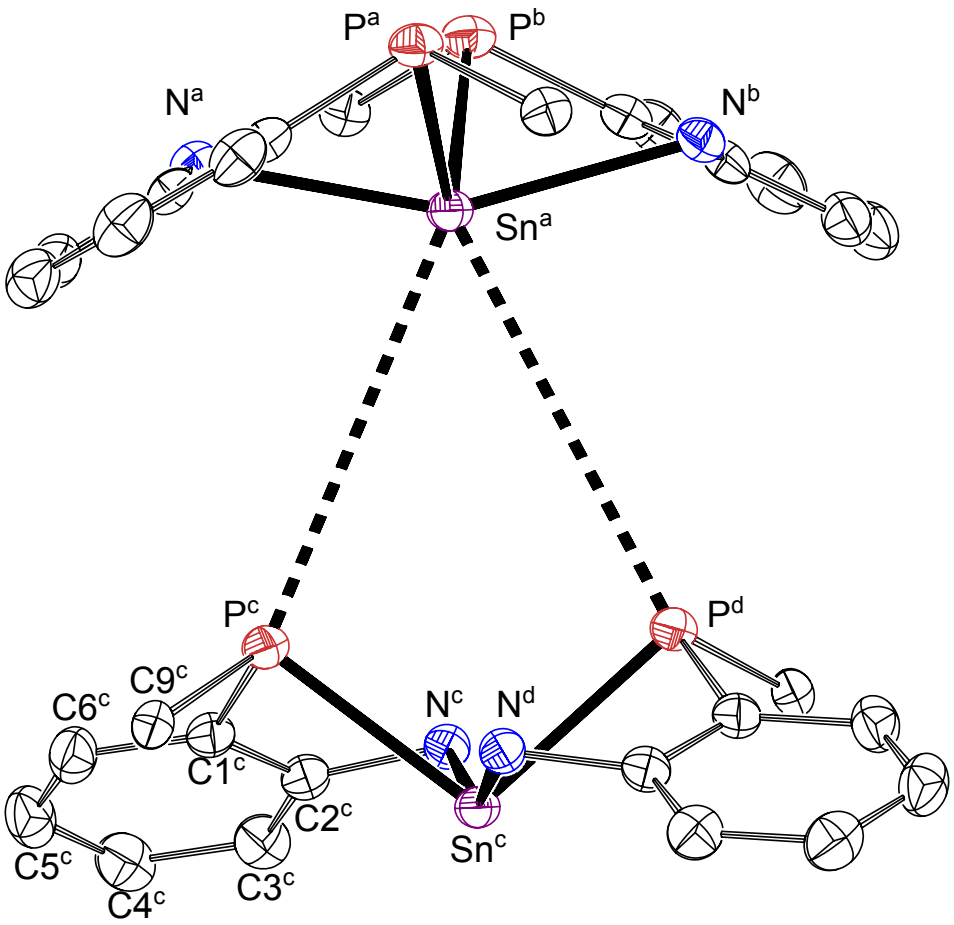

Figure S12: Two molecules of **2** crystallized from *n*-hexane, **2(hex)**; hydrogen atoms, phenyl carbons except for ipso and methyl groups have been omitted. The superscripts to the atom labels correspond to the following symmetry operations: *a* ($\frac{3}{2}-$y, $\frac{1}{2}-$y, z); *b* (x, y, z); *c* (1$-$y, $-\frac{1}{2}+$x, $-\frac{1}{2}+$z); *d* ($\frac{1}{2}+$y, 1$-$x, $-\frac{1}{2}+$z).

2 Computational Details and Theoretical Data

The Amsterdam density functional (ADF)[11] code was used for the NMR calculations and the Turbomole package[12] for geometry optimizations. Considering the large size of the system and the presence of heavy elements (Sn), the employment of the DFT approach seems to be a reasonable choice. The hybrid functional PBE0 was employed as it is known for good performance in calculating NMR properties for molecules also containing electron-rich atoms.[13] The presence of heavy atoms requires also to include relativistic corrections to the quantum chemical calculations, which was done using both scalar and spin-orbit approaches for the NMR properties. The relativistic effects for the NMR calculations are considered by means of the two-component zeroth-order regular approximation (ZORA, scalar-only or scalar + spin-orbit relativistic effects) method.[14]

2.1 Magnetic Shielding Tensors

The geometries of the monomer of **2** and of the reference systems PH_3 and $SnMe_4$ were optimized at the PBE0-D3/def2-QZVP level of theory. In the case of **2**, the optimization started from the X-ray data obtained for **2(thf)** and **2(hex)** and converged to the same structure in C_1, reported in Table S1. The nuclear coordinates and magnetic shielding tensors for PH_3 are given in Table S2, and in Table S3 for $SnMe_4$.

Chemical shifts were obtained according to:[15]

$$\delta(\mathrm{X}) = \frac{\sigma(\mathrm{ref}) - \sigma(\mathrm{X})}{1 - \sigma(\mathrm{ref})} \approx \sigma(\mathrm{ref}) - \sigma(\mathrm{X}) \tag{S1}$$

where $\sigma(\mathrm{ref})$ is the magnetic shielding of the nucleus in the reference compound and $\sigma(\mathrm{X})$ the magnetic shielding of the nucleus in the compound of interest. In the present study, the approximation in eq. S1 has been used in order to be consistent with the majority of NMR computational studies.[16] This approximation introduces errors of up

to 3 ppm in the ^{119}Sn chemical shifts. Nevertheless, these deviations ($\approx$ 0.6% of 530 ppm) are smaller than typical errors of quantum chemical NMR calculations ($\approx$ 10%) and can be therefore neglected.

For ^{119}Sn, the reference compound is $SnMe_4$; its calculated magnetic shieldings are listed in Tables S3 and S4.[17] For ^{31}P, the primary reference compound is 85% aq. H_3PO_4, but for the calculations the more suitable phosphine PH_3 was selected as secondary reference, with a chemical shift $\delta(^{31}P)$ = –266.1 ppm wrt. 85% aq. H_3PO_4.[18] In principle, this change of reference compound in eq. S1 needs to consider the change in the chemical shift standard as well:[19]

$$\delta = \delta' \frac{\nu_{\mathrm{ref}'}}{\nu_{\mathrm{ref}}} + \frac{\nu_{\mathrm{ref}'} - \nu_{\mathrm{ref}}}{\nu_{\mathrm{ref}}} = \delta'(1 + \delta_{\mathrm{ref}'}) + \delta_{\mathrm{ref}'} \approx \delta' + \delta_{\mathrm{ref}'} \tag{S2}$$

where $\delta_{\mathrm{ref}'}$ denotes the chemical shift of the secondary reference with respect to the primary reference, δ' the chemical shift of the compound with respect to the secondary reference, and δ the chemical shift with respect to the primary reference. However, for ^{31}P the deviation is less than 0.1 ppm if the approximation in eq. S2 is used instead.

Table S1: Nuclear Coordinates and Magnetic Shielding Tensors for $Sn(NP)_2$, **2**, optimized in C_1.

atom	x/Å	y/Å	z/Å
C(1)	5.2956	8.1647	4.5721
C(2)	5.4545	8.9511	2.3180
C(3)	6.8287	11.3936	3.6040
C(4)	5.5377	13.9053	3.4192
C(5)	8.0274	12.0692	3.8390
C(6)	5.2650	14.9699	2.5592
C(7)	6.7383	10.0531	4.0141
C(8)	5.4527	16.5431	4.3662
C(9)	5.2123	16.2754	3.0280
C(10)	8.9754	10.1495	4.9122
C(11)	7.8053	9.4489	4.6691
C(12)	5.7891	14.1942	4.7644
C(13)	5.7508	15.4967	5.2308
C(14)	9.0886	11.4632	4.4873
C(15)	2.1242	14.0947	4.5721
C(16)	1.9653	13.3083	2.3180
C(17)	0.5911	10.8658	3.6040
C(18)	1.8821	8.3541	3.4192
C(19)	–0.6075	10.1901	3.8391
C(20)	2.1547	7.2895	2.5592
C(21)	0.6815	12.2063	4.0140
C(22)	1.9670	5.7162	4.3662
C(23)	2.2074	5.9839	3.0279
C(24)	–1.5556	12.1099	4.9122
C(25)	–0.3855	12.8105	4.6691
C(26)	1.6307	8.0651	4.7644
C(27)	1.6690	6.7627	5.2307
C(28)	–1.6688	10.7962	4.4873
H(29)	4.2968	7.7813	4.3750
H(30)	6.0119	7.3611	4.3649
H(31)	5.3635	8.4441	5.6225
H(32)	4.4896	8.4893	2.1199
H(33)	5.5591	9.8270	1.6802
H(34)	6.2501	8.2361	2.0763
H(35)	8.1174	13.1010	3.5225
H(36)	5.0949	14.7677	1.5074
H(37)	5.4163	17.5607	4.7346

Contd. on next page

Table S1 – contd. from previous page

H(38)	4.9927	17.0847	2.3422
H(39)	9.7944	9.6645	5.4279
H(40)	7.7296	8.4219	4.9981
H(41)	6.0108	13.3856	5.4506
H(42)	5.9444	15.6971	6.2777
H(43)	10.0003	12.0200	4.6645
H(44)	3.1230	14.4782	4.3750
H(45)	1.4078	14.8983	4.3648
H(46)	2.0563	13.8153	5.6225
H(47)	2.9302	13.7701	2.1199
H(48)	1.8607	12.4324	1.6802
H(49)	1.1698	14.0233	2.0763
H(50)	–0.6975	9.1583	3.5227
H(51)	2.3249	7.4917	1.5074
H(52)	2.0035	4.6986	4.7346
H(53)	2.4270	5.1747	2.3422
H(54)	–2.3747	12.5950	5.4278
H(55)	–0.3098	13.8375	4.9981
H(56)	1.4091	8.8738	5.4506
H(57)	1.4753	6.5623	6.2777
H(58)	–2.5804	10.2393	4.6646
Sn(59)	3.7099	11.1297	4.3823
P(60)	5.4373	12.2080	2.7350
P(61)	1.9825	10.0513	2.7350
N(62)	5.5245	9.3356	3.7327
N(63)	1.8953	12.9238	3.7327

^{119}Sn magnetic shielding for Sn(59)

Cartesian representation

2208.014	–125.039	5.909
–125.039	2172.114	–6.251
5.909	–6.251	2807.007

principal components

2063.742	2316.236	2807.157

principal axis system

0.655	0.756	0.012
0.756	–0.655	–0.012
0.001	–0.017	1.000

^{31}P magnetic shielding for P(60)

Cartesian representation

344.607	–56.331	–2.792

Contd. on next page

Table S1 – contd. from previous page

–56.331	442.667	15.118
–2.792	15.118	362.465
principal components		
318.629	360.729	470.380
principal axis system		
0.903	0.137	0.407
0.421	–0.088	–0.903
–0.088	0.987	–0.137
^{31}P magnetic shielding for P(61)		
Cartesian representation		
342.294	–56.986	1.277
–56.986	443.350	–18.740
1.277	–18.740	360.826
principal components		
315.675	359.009	471.786
principal axis system		
0.895	–0.201	0.399
0.421	0.081	–0.903
0.150	0.976	0.157

2.2 Spin-Spin Coupling Constants

2.2.1 Comparison to Experiment

For the calculation of the spin-spin coupling constants, two molecules of **2** crystallized from *n*-hexane, **2(hex)**, or crystallized from THF, **2(thf)**, were taken from the X-ray structures (see Figures S12 and S10) without any additional geometry optimization.

There are four terms contributing to the total spin-spin coupling constant *J*(X,X′): the Fermi-contact (FC), diamagnetic spin-orbit (DSO), paramagnetic spin-orbit (PSO), and spin-dipole (SD). The total coupling constant is given by Eq. S3:[20]

$$J(\mathrm{X},\mathrm{X}') = {}^{\mathrm{FC}}J(\mathrm{X},\mathrm{X}') + {}^{\mathrm{DSO}}J(\mathrm{X},\mathrm{X}') + {}^{\mathrm{PSO}}J(\mathrm{X},\mathrm{X}') + {}^{\mathrm{SD}}J(\mathrm{X},\mathrm{X}') \tag{S3}$$

Table S2: Nuclear Coordinates and ^{31}P Magnetic Shielding Tensor for PH_3

atom	x/Å	y/Å	z/Å
P(1)	–1.8446	0.1202	0.0000
H(2)	–1.0721	–1.0699	0.0000
H(3)	–1.0736	0.7162	1.0312
H(4)	–1.0736	0.7162	–1.0312
^{31}P magnetic shielding			
Cartesian representation			
	546.786	−0.072	0.000
	−0.072	611.599	0.000
	0.000	0.000	611.632
principal components			
	546.786	611.599	611.632
principal axis system			
	1.000	−0.001	0.000
	0.001	1.000	0.000
	0.000	0.000	1.000

Within the ZORA approximation the FC, SD, and PSO terms contain cross terms with the others. In this work we report the DSO, the PSO, and the total FC + SD term. Table S5 collects the experimental and calculated spin-spin coupling constants. The agreement between experiment and calculations is acceptable, taking into account that the computational model does not include any crystal effects, which makes the comparison with solid-state NMR experiment more difficult. Nevertheless, the magnitudes are reproduced by the calculations quite well.

2.2.2 Dependence on Method

In order to assess the basis set dependence of the calculated spin-spin coupling constants, different methods have been used and the results are summarized and compared to experimental values in Table S6. As expected, the chosen DFT approach and the inclusion of the JCPL basis set parametrized for the coupling constant calculations (not available for the Sn atom) do have influence on the calculated values. Never-

Table S3: Nuclear Coordinates and ^{119}Sn Magnetic Shielding Tensor for $SnMe_4$

atom	x/Å	y/Å	z/Å
Sn(1)	–1.3223	–0.2703	0.0000
C(2)	–0.6069	0.7416	–1.7525
C(3)	–3.4686	–0.2703	0.0000
C(4)	–0.6069	0.7416	1.7525
C(5)	–0.6071	–2.2939	0.0000
H(6)	–0.9638	1.7713	–1.7679
H(7)	0.4829	0.7517	–1.7661
H(8)	–0.9608	0.2380	–2.6520
H(9)	–3.8477	–0.7812	–0.8851
H(10)	–3.8477	–0.7814	0.8849
H(11)	–3.8479	0.7515	0.0001
H(12)	–0.9624	0.2392	2.6520
H(13)	0.4829	0.7499	1.7671
H(14)	–0.9622	1.7719	1.7669
H(15)	0.4827	–2.3109	–0.0001
H(16)	–0.9624	–2.8216	0.8850
H(17)	–0.9625	–2.8217	–0.8850

^{119}Sn magnetic shielding

Cartesian representation

2936.524	0.033	0.003
0.033	2936.674	−0.002
0.003	−0.002	2936.703

principal components

2936.517	2936.681	2936.703

principal axis system

0.978	0.209	0.002
−0.208	0.975	−0.078
−0.018	0.075	0.997

Table S4: Principal Components[a] of the ^{31}P and ^{119}Sn NMR Magnetic Shielding ($T = \sigma$) and Chemical Shift Tensors ($T = \delta$) of Compound **2** and the Reference Compounds PH_3 and $SnMe_4$.

nucleus	T	compound	T_{iso}/ppm	T_{11}/ppm	T_{22}/ppm	T_{33}/ppm	Ω/ppm	κ
^{31}P	σ	PH_3 calc.	590.0	546.8	611.6	611.6	64.8	–1.00
		2 calc.[b]	383.3	319.2	360.4	470.4	151.2	0.45
			383.4	316.9	360.5	472.8	155.9	0.44
	δ	**2** calc[b,c]	–59.4	4.7	–36.5	–146.5	151.2	0.45
			–59.5	7.0	–36.6	–148.9	155.9	0.44
		2(thf) exp.	–55.1	23	–39	–149	171	0.27
		2(hex) exp.	-60.7	–6	–28	–148	143	0.69
^{119}Sn	σ	$SnMe_4$ calc.	2936.6	2936.5	2936.6	2936.7	0.2	–0.83
		2 calc.	2407.0	2083.4	2320.4	2817.3	733.9	0.35
	δ	**2** calc.[d]	529.6	853.2	616.2	119.3	733.9	0.35
		2(thf) exp.	472	802	532	82	720	0.25
		2(hex) exp.	356	612	608	–158	770	0.98

[a] $\sigma_{11} \leq \sigma_{22} \leq \sigma_{33}$; $\delta_{11} \geq \delta_{22} \geq \delta_{33}$; isotropic value T_{iso}= $(T_{11}+T_{22}+T_{33})/3$; span $\Omega \approx \sigma_{33} - \sigma_{11} \approx \delta_{11} - \delta_{33}$; skew κ= $3(\delta_{22} - \delta_{iso})/\Omega$; $-1 \leq \kappa \leq 1$. [b] Structure optimized in C_1. [c] Chemical shifts wrt. 85% aq. H_3PO_4 using the calculated magnetic shielding of PH_3, see text. [d] Chemical shifts wrt. the calculated magnetic shielding of $SnMe_4$.

Table S5: Calculated[a] and Experimental Spin-Spin Coupling Constants (in Hz) Determined for Dimers of Compound **2**. Labelling Corresponds to Fig. S10 and S12.

property	structure	DSO	PSO[b]	FC+SD[c]	total	exp.[d]
$^1J(^{119}Sn^c,^{31}P^{c,d})$ ("endo")	**2(thf)**	–0.4	42.8	701.4	743.9	845
	2(hex)	–0.4	40.1	688.4	728.1	816
$^1J(^{119}Sn^a,^{31}P^{a,b})$ ("exo")	**2(thf)**	–0.4	43.0	725.4	768.0	
	2(hex)	–0.4	40.1	709.7	749.5	
$^{TS}J(^{119}Sn^a,^{31}P^{c,d})$	**2(thf)**	–0.3	0.7	–305.9	–305.4	263
	2(hex)	–0.2	0.8	–290.4	–289.8	277
$^2J(^{31}P^c,^{31}P^d)$ ("endo")	**2(thf)**	0.2	0.9	37.1	38.2	+45
	2(hex)	0.2	1.1	46.3	47.6	n.d.
$^2J(^{31}P^a,^{31}P^b)$ ("exo")	**2(thf)**	0.1	1.2	48.3	49.6	
	2(hex)	0.1	1.4	60.3	61.8	

[a] PBE0/QZ4P + relativistic corrections, using first-order VWN potential for coupling constants calculations. [b] With FC + SD cross terms. [c] With PSO cross terms. [d] Except for $^2J(^{31}P,^{31}P)$, the signs of the coupling constants have not been determined.

theless, the mean absolute deviations (MADs) of all tested approaches with respect to experiment are similar.

Table S6: Experimental and Calculated $^{1}J(^{119}\mathrm{Sn},^{31}\mathrm{P})$, $^{TS}J(^{119}\mathrm{Sn},^{31}\mathrm{P})$, and $^{2}J(^{31}\mathrm{P},^{31}\mathrm{P})$ Spin-Spin Coupling Constants in a Dimer of **2(thf)** Calculated Using Different Theoretical Approaches.

	M1[a]	M2[b]	M3[c]	exp.[d]
$^{1}J(^{119}\mathrm{Sn}^{c},^{31}\mathrm{P}^{c,d})$	743.9	848.8	772.3	845
$^{TS}J(^{119}\mathrm{Sn}^{a},^{31}\mathrm{P}^{c,d})$	–305.4	–415.3	–317.4	263
$^{2}J(^{31}\mathrm{P}^{c},^{31}\mathrm{P}^{d})$	38.2	50.4	40.1	+45
MAD[e]	50.1	53.8	44.0	

[a] M1: PBE0-ZORA-SO/QZ4P using first-order VWN potential. [b] M2: PBE0-ZORA-SO/QZ4P/JCPL(P) using first-order GGA potential. The JCPL basis set was used for the P atoms and the QZ4P basis set was used for all other atoms. [c] M3: PBE0-ZORA-SO/QZ4P/JCPL(P) using first-order VWN potential. The JCPL basis set was used for the P atoms and the QZ4P basis set was used for all other atoms. [d] Except for $^{2}J(^{31}\mathrm{P},^{31}\mathrm{P})$, the signs of the coupling constants have not been determined. [e] Mean absolute deviation with respect to experiment.

2.2.3 Dependence on Intermolecular Distance

The large value of the $^{TS}J(^{119}\mathrm{Sn}^{a},^{31}\mathrm{P}^{c,d})$ coupling constant in spite of a huge interatomic distance, Sn^{a}–$\mathrm{P}^{c,d}$ = 4.7 Å, raises the question about the dependence of this coupling constant on the distance between the $[\mathrm{Sn(NP)_2}]$ fragments. The dependence of the through-space coupling between the $[\mathrm{Sn(NP)_2}]$ fragments on the distance between the fragments was studied using two complexes with varying Sn^{a}–$\mathrm{P}^{c,d}$ distances. Because such a large series of calculations is very expensive computationally for the complete dimer, a simplified model system was used. In this model system, ethylenediyl fragments replace the aromatic rings bridging the phosphorus and nitrogen atoms and hydrogen atoms replace the phenyl and methyl groups (Fig. S13).

The value of $^{TS}J(^{119}\mathrm{Sn}^{a},^{31}\mathrm{P}^{c,d})$ calculated for the simplified system at the experimental Sn^{a}–$\mathrm{P}^{c,d}$ distance of 4.6866(5) Å corresponds to –382 Hz, which is comparable

to the value calculated for the full system, –289.8 Hz (Tab. S5).

Table S7 collects the data used for the J vs. distance plot, Fig. S14: the total calculated coupling constants and the individual contributions (FC + SD, PSO and DSO). One can see that the DSO and PSO contributions are relatively minor, and the coupling mechanism is dominated by FC + SD term.

Table S7: Calculated Spin-Spin Couplings $^{1}J(^{119}Sn^{c},^{31}P^{c,d})$ and $^{TS}J(^{119}Sn^{a},^{31}P^{c,d})$ vs. Intermolecular Distances r Between Two [$Sn(NP)_2$] Fragments.[a] Level of Theory: PBE0/TZ2P + Relativistic Corrections, Using First-Order VWN Potentials.

$r(Sn^{a},Sn^{c})$	4.89	5.29	5.49	5.69	5.893	6.09	6.29	6.49	6.69	6.89	7.09
$r(Sn^{a},P^{c,d})$	3.807	4.151	4.327	4.504	4.687	4.865	5.047	5.231	5.416	5.602	5.788
$^{1}J(^{119}Sn^{c},^{31}P^{c,d})$											
Total	614.2	599.9	596.1	594.0	592.7	592.3	591.0	590.6	589.8	589.0	588.2
FC+SD[b]	571.7	559.5	556.0	553.9	552.5	551.9	550.5	550.0	549.1	548.2	547.4
PSO[c]	42.7	40.6	40.3	40.3	40.4	40.6	40.7	40.8	40.9	41.0	41.0
DSO	–0.2	–0.2	–0.2	–0.2	–0.2	–0.2	–0.2	–0.2	–0.2	–0.2	–0.2
$^{TS}J(^{119}Sn^{a},^{31}P^{c,d})$											
Total	–1556.2	–948.9	–712.5	–528.0	–382.1	–274.9	–194.4	–134.6	–93.3	–64.1	–43.7
FC+SD[b]	–1561.1	–951.0	–713.8	–528.7	–382.6	–275.1	–194.5	–134.6	–93.2	–64.0	–43.6
PSO[c]	5.1	2.3	1.5	0.9	0.6	0.3	0.2	0.1	0.0	0.0	0.0
DSO	–0.2	–0.2	–0.2	–0.2	–0.1	–0.1	–0.1	–0.1	–0.1	–0.1	–0.1

[a] Based on structure **2(hex)**, cf. Fig. S12, but with an ethylenediyl fragment replacing the aromatic rings bridging phosphorus and nitrogen and hydrogen atoms instead of the phenyl and methyl groups, cf. Fig S13. The column corresponding to experimental distances is highlighted. [b] With PSO cross terms. [c] With FC + SD cross terms.

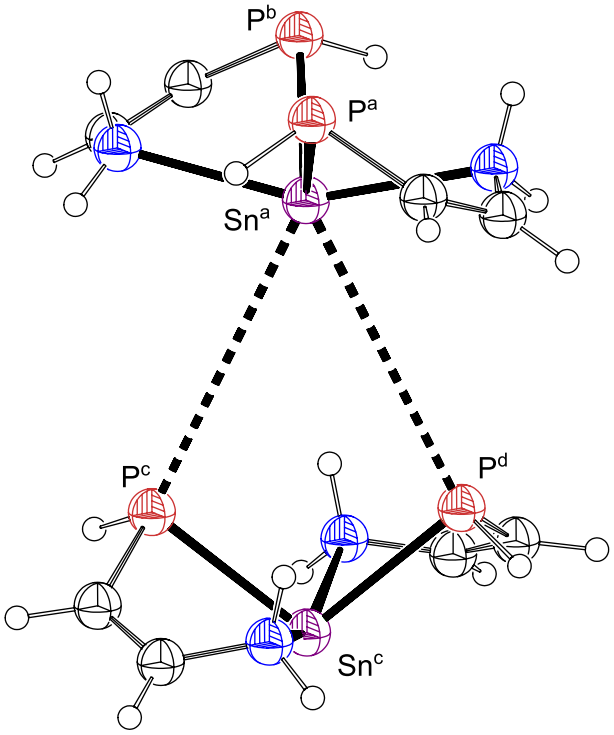

Figure S13: The model system for the "scan" calculations.

2.2.4 NBO Analysis

In order to gain some insight into the nature of the intermolecular interaction, displayed by the through-space spin-spin coupling constant $^{TS}J(^{119}Sn^{a},^{31}P^{c,d})$, the electrostatic potential surface of **2(hex)** was considered (Figure S15). The negatively charged area located at the phosphorus atoms and the positive potential at the tin atom determine the electrostatic interaction between the two [Sn(NP)$_2$] fragments. The NBO analysis of two molecules of **2** indicates no covalent interaction between the [Sn(NP)$_2$] fragments.

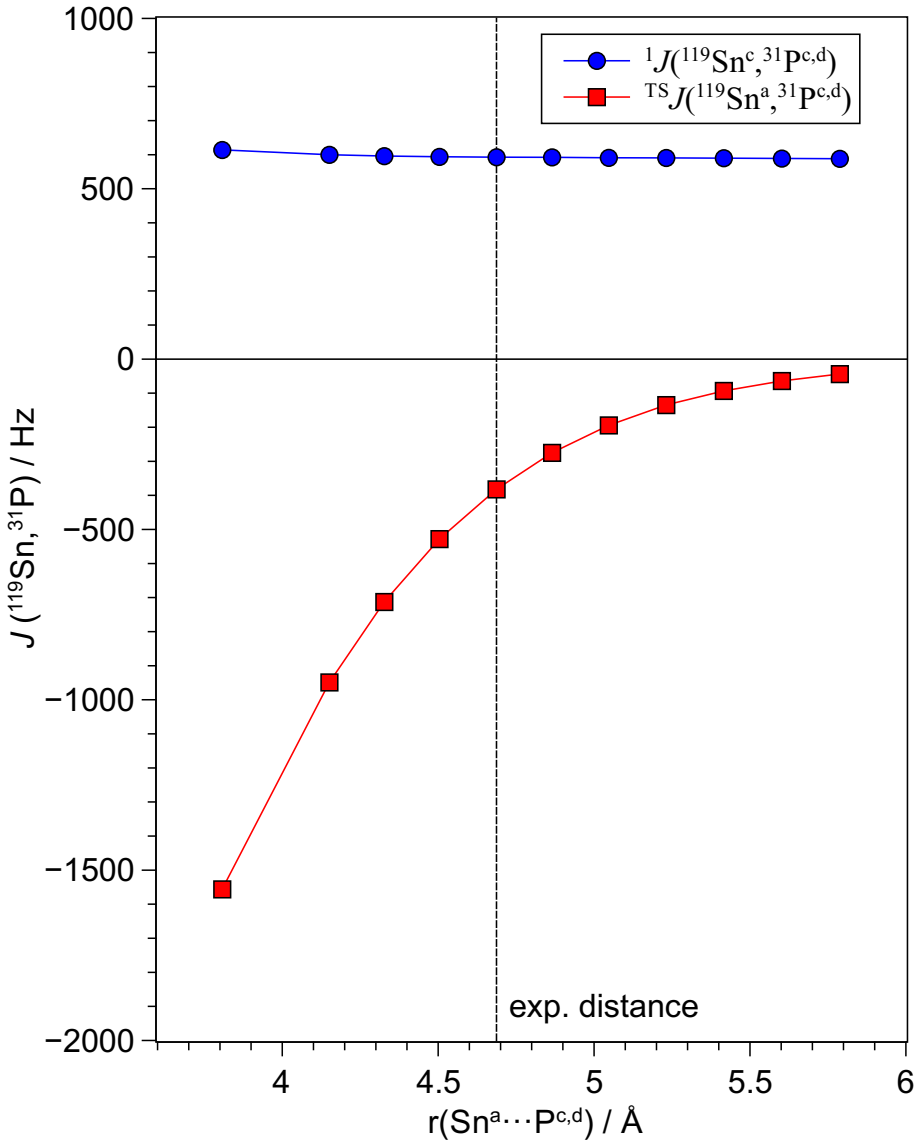

Figure S14: Calculated dependence of $^{1}J(^{119}\mathrm{Sn}^{c},^{31}\mathrm{P}^{c,d})$ and $^{TS}J(^{119}\mathrm{Sn}^{a},^{31}\mathrm{P}^{c,d})$ on the intermolecular $\mathrm{Sn}^{a}\cdots\mathrm{P}^{c,d}$ distances in the model system (cf. Fig. S13).

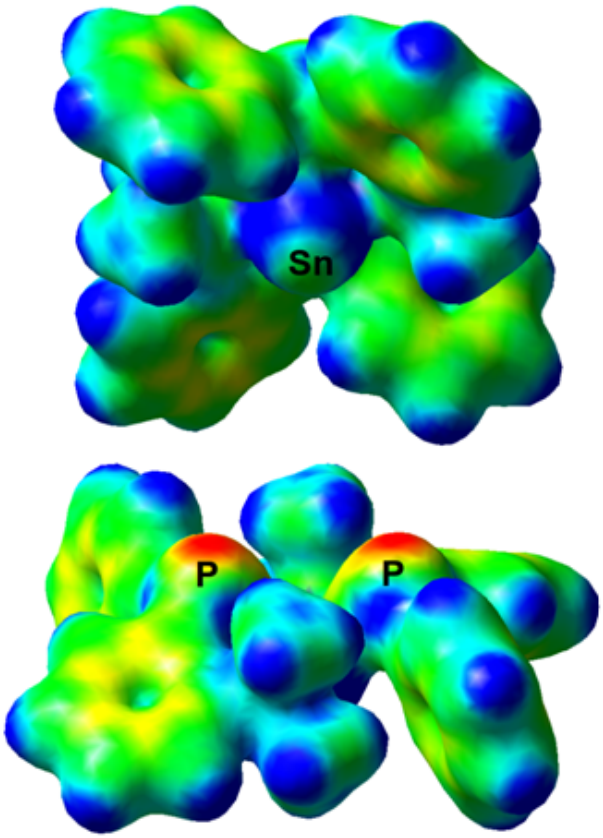

Figure S15: MEP on the 0.02 au electron density isosurface. Color code (au): blue > 0.11 > –0.02 > red. Level of theory: PBE0/TZ2P + relativistic corrections.

References

(1) Arras, J.; Eichele, K.; Wesemann, L. *Eur. J. Inorg. Chem.* **2013**, 5728–5737.

(2) Harris, R. K.; Becker, E. D.; Cabral de Menezes, S. M.; Goodfellow, R.; Granger, P. *Pure Appl. Chem.* **2001**, *73*, 1795–1818.

(3) Bryce, D. L.; Bernard, G. M.; Gee, M.; Lumsden, M. D.; Eichele, K.; Wasylishen, R. E. *Can. J. Anal. Sci. Spectrosc.* **2001**, *46*, 46–82.

(4) Izod, K.; Stewart, J.; Clegg, W.; Harrington, R. W. *Organometallics* **2010**, *29*, 108–116.

(5) SAINT, APEX2, Bruker AXS Inc., Madison, 2007.

(6) SADABS, University of Göttingen, Germany, 2008.

(7) Farrugia, L. *J. Appl. Cryst.* **1999**, *32*, 837–838.

(8) X-AREA v. 1.26, Stoe & Cie GmbH, 2004.

(9) SHELXS 97, Göttingen, Germany, 1997.

(10) SHELXL 97, Göttingen, Germany, 1997.

(11) te Velde, G.; Bickelhaupt, F. M.; Baerends, E. J.; Fonseca Guerra, C.; van Gisbergen, S. J. A.; Snijders, J. G.; Ziegler, T. *J. Comput. Chem.* **2001**, *22*, 931–967.

(12) Ahlrichs, R.; Armbruster, M. K.; Bär, M.; Baron, H.-P.; Bauernschmitt, R.; Crawford, N.; Deglmann, P.; Ehrig, M.; Eichkorn, K.; Elliott, S.; Furche, F.; Haase, F.; Häser, M.; Hättig, C.; Hellweg, A.; Horn, H.; Huber, C.; Huniar, U.; Kattannek, M.; Kölmel, C.; Kollwitz, M.; May, K.; Nava, P.; Ochsenfeld, C.; Öhm, H.; Patzelt, H.; Rappoport, D.; Rubner, O.; Schäfer, A.; Schneider, U.; Sierka, M.; Treutler, O.;

Unterreiner, B.; von Arnim, M.; Weigend, F.; Weis, P.; Weiss, H. TURBOMOLE, Universität Karlsruhe and Forschungszentrum Karlsruhe GmbH: Karlsruhe, Germany; http://www.turbomole.com.

(13) (a) Adamo, C.; Barone, V. *Chem. Phys. Lett.* **1998**, *298*, 113–119; (b) Adamo, C.; Barone, V. *J. Chem. Phys.* **1999**, *110*, 6158–6170; (c) Grimme, S.; Antony, J.; Ehrlich, S.; Krieg, H. *J. Chem. Phys.* **2010**, *132*, 154104.

(14) (a) van Lenthe, E.; Baerends, E. J.; Snijders, J. G. *J. Chem. Phys.* **1993**, *99*, 4597–4610; (b) van Lenthe, E.; Baerends, E. J.; Snijders, J. G. *J. Chem. Phys.* **1994**, *101*, 9783–9792; (c) van Lenthe, E.; van Leeuwen, R.; Baerends, E. J.; Snijders, J. G. *Int. J. Quantum Chem.* **1996**, *57*, 281–293; (d) van Lenthe, E.; Snijders, J. G.; Baerends, E. J. *J. Chem. Phys.* **1996**, *105*, 6505–6516; (e) van Lenthe, E.; Ehlers, A.; Baerends, E.-J. *J. Chem. Phys.* **1999**, *110*, 8943–8953.

(15) Mason, J. *Solid State Nucl. Magn. Reson.* **1993**, *2*, 285–288.

(16) (a) Ruiz-Morales, Y.; Schreckenbach, G.; Ziegler, T. *J. Phys. Chem. A* **1997**, *101*, 4121–4127; (b) Bayse*, C. A. *J. Chem. Theory Comput.* **2005**, *1*, 1119–1127; (c) Vivas-Reyes, R.; Proft, F. D.; Biesemans, M.; Willem, R.; Geerlings, P. *J. Phys. Chem. A* **2002**, *106*, 2753–2759; (d) Bühl, M.; Wrackmeyer, B. *Magn. Reson. Chem.* **2010**, *48*, S61–S68.

(17) van Wüllen, C. *Phys. Chem. Chem. Phys.* **2000**, *2*, 2137–2144.

(18) Jameson, C. J.; De Dios, A.; Keith Jameson, A. *Chem. Phys. Lett.* **1990**, *167*, 575–582.

(19) Kidd, R. G.; Goodfellow, R. J. In *NMR and the Periodic Table*; Harris, R. K., Mann, B. E., Eds.; Academic Press, London, 1978; pp 195–278.

(20) Ramsey, N. F. *Phys. Rev.* **1953**, *91*, 303–307.